Liquid microstructures at solid interfaces

Stephan Herminghaus†, Andreas Fery‡, Stefan Schlagowski†, Karin Jacobs†, Ralf Seemann†, Hartmut Gau‡, Wolfgang Mönch† and Tilo Pompe‡

† Universität Ulm, Abb. Angewandte Physik, 89069 Ulm, Germany
‡ MPI für Kolloid- und Grenzflächenforschung, 14424 Potsdam-Golm, Germany

Abstract. The propensity of liquid films to bead off poorly wettable substrates leads to a wide variety of liquid structures via mechanisms which are far from being fully understood. In particular, dewetting via unstable surface waves may be driven at least by dispersion forces, electrostatic forces, or by Marangoni-type transport. A hierarchy of dynamical instabilities finally transforms the initial homogeneous film into the final state, consisting of an ensemble of individual, isolated droplets. While these processes of self-organized structure formation are interesting in themselves, it may also be desirable to generate liquid structures in a more well-defined and predictable way. We have therefore investigated experimentally the behaviour of various liquids on substrates, the wettability of which has been laterally structured. The resulting artificial liquid objects display several remarkable properties, both statically and dynamically. Aside from potential applications as 'liquid microchips', it is shown how fundamental quantities can be extracted from the shapes of the liquid surfaces, as determined by scanning force microscopy. The three-phase contact line tensions obtained in this way are in fair agreement with theoretical predictions and might help to resolve long-standing debates on the role of wetting forces on the nanometre scale.

1. Introduction

Under what circumstances, and in which morphology, is a substance thermodynamically stable at the surface of a given material? This question defines the field of research of wetting phenomena. If the substance, which henceforth will be assumed to be liquid, wets the substrate completely, the answer is comparably simple and tractable: it forms a continuous film at the interface, with parallel, flat boundaries if the interface is smooth. While the determination of the detailed morphology and transport behaviour of such homogeneous films already poses substantial challenges for both theorists and experimentalists, the behaviour of the liquid in the non-wetting case is tremendously more complex. Since in this case the liquid tends to form a finite angle with the substrate, a stable state with a translational invariance parallel to the interface does not exist anymore. As a consequence, there is a wide variety of shapes the liquid may assume, with a complicated dynamics of transforming one into the other on the way to thermal equilibrium.

The present study summarizes our recent contributions to understanding the various mechanisms of structure formation in liquids at solid interfaces. On the time scales that the various instabilities take place, the fluids used here may be safely considered as nonvolatile, such that shape transformations proceed at constant volume. In the first section, several mechanisms of spontaneous symmetry breaking in thin liquid films on homogeneous surfaces are presented, which lead to the formation of individual, isolated droplets out of a homogeneous film. In the second section, strategies will be discussed to tame these instabilities in order to

form liquid structures at small scales in a more predictable and controlled manner. Possible applications will be discussed briefly. In the third section, it will be shown how such liquid structures, when scaled down to the nanometre regime, may yield substantial insight into fundamental forces in wetting science, which perhaps will allow long-standing debates in the field to be resolved.

2. Self-organized structure formation: dewetting of homogeneous substrates

Suppose we have deposited a thin homogeneous film onto a substrate or interface which is not wetted by the film material. The latter will then seek to establish the finite contact angle which the substrate thermal equilibrium requires, and at the same time to minimize its total free energy. In other words, it will bead off the substrate and form an ensemble of individual droplets which may have different volumes, but for which the angle of contact they form with the substrate at their boundaries is the same. This is in some sense analogous to decomposition processes, in which a formerly homogeneous composition decays into a complex interconnected structure of 'rich' and 'dilute' phase regions. Just as one may have decomposition by heterogeneous nucleation as well as by dynamically unstable composition fluctuations, the rupture of a homogeneous thin film may be initiated by nucleation of holes from defects, as well as by amplification of unstable fluctuations in film thickness. The latter process is also frequently referred to as a 'spinodal' process.

Nucleation is considered the more 'common' reason for adhesion failure of a liquid film, because a very small amount of defects (i.e. dirt particles) is necessary to induce dewetting. However, spinodal dewetting, or dewetting by unstable thickness undulations is particularly interesting since it represents a true spontaneous symmetry breaking and structure formation process. Furthermore, the number of systems in which this is observed has recently continued to increase. We will thus concentrate here on this scenario, as far as the initial stages of dewetting are concerned.

If the long-range forces across a wetting layer, such as the van der Waals force, are in favour of wetting, they act as the principal restoring forces of lateral film thickness fluctuations, i.e., of thermally activated surface waves. Their amplitude is usually small compared to the film thickness, such that thermally activated nucleation of dry patches can be safely neglected. If, however, the long range forces are in disfavour of wetting, they represent a driving force for thickness fluctuations, whose amplitude is thus expected to grow exponentially in time [1–4]. In the valleys of these fluctuations, the liquid surface finally reaches the substrate and initiates dewetting [4–6].

The conditions for this to occur can be conveniently expressed in terms of the effective interaction potential of the film, $\Phi(h)$, which describes the interaction of the solid/liquid interface with the liquid/air interface [7, 8]. It is defined as the excess free energy which is necessary to approach these two interfaces from infinity to the film thickness, l. For dewetting to occur, the global minimum of Φ must be at finite l, which then represents the equilibrium film thickness. It is readily shown that if the second derivative of Φ with respect to l is negative, unstable modes exist whose amplitude grows exponentially according to $\exp(t/T)$. Furthermore, there is a characteristic wave number, q_m, for which T^{-1} attains a maximum. The corresponding mode grows the fastest and is thus expected to dominate the emerging dewetting structure.

Let us start with the consideration of liquid crystal (LC) films, which turn out to be quite powerful model systems for this kind of effect. In our experiments, thin films of $5AB_4$ (tris(trimethylsiloxy)silane-ethoxy-cyanobiphenyl) [9] were used. This material undergoes a phase transition from the crystalline into the isotropic state at $18\,^\circ$C. Films of $5AB_4$ were
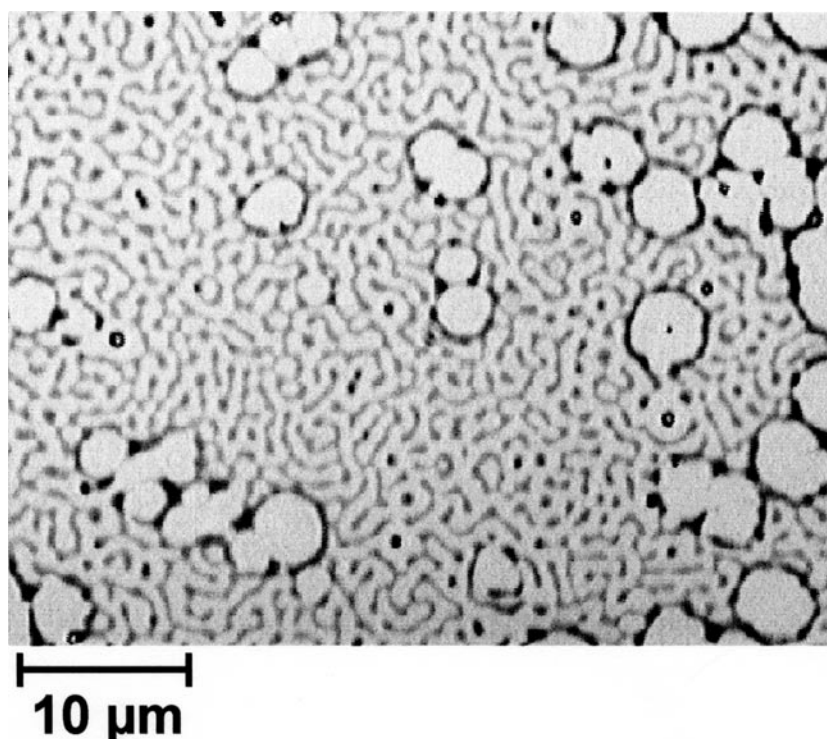
Figure 1. Optical micrograph of a patch of 5AB$_4$ at room temperature, after transfer from the Langmuir trough to a silicon wafer. Both circular holes nucleated from defects, and an undulative mode indicating spinodal dewetting are clearly distinguished.

prepared by spreading the material from chloroform solution onto the surface of deionized water in a Langmuir trough at 10 °C. By surface compression, films with a typical thickness of $l = 40$ nm could easily be formed [9]. They were transferred at a surface pressure of 6.9 mN m^{-1} onto silicon wafers which had been cleaned and hydrophilized by a modified 'RCA procedure' [10].

The LC film dewets in the course of several minutes (cf figure 1), involving various dewetting mechanisms. On the one hand, circular 'dry' holes appear, the rims of which are formed by the material removed from the hole. This is characteristic of nucleation from defects in the film, some of which are visible in the centres of the holes. In addition, dewetting by an undulative mode occurs across the patch, which exhibits a clearly defined critical wavelength, as expected for spinodal dewetting. When the dewetting process is inspected through the light microscope, one observes the nucleated dewetting to start almost immediately and to proceed gradually with time. In contrast, the undulative mode is not visible in the beginning, but appears after some time (several seconds to minutes), then rapidly grows in amplitude until it reaches the state shown in figure 1. This is the behaviour expected for a dynamically unstable mode. It should be noted that the presence of the circular holes demonstrates that the system is really nonwetting.

The spinodal dewetting in this system may be qualitatively understood from the molecular interactions. The LC molecules are strongly dipolar, and thus a strongly polar substrate is required to prepare homogeneous films (complete wetting); otherwise there would be dewetting
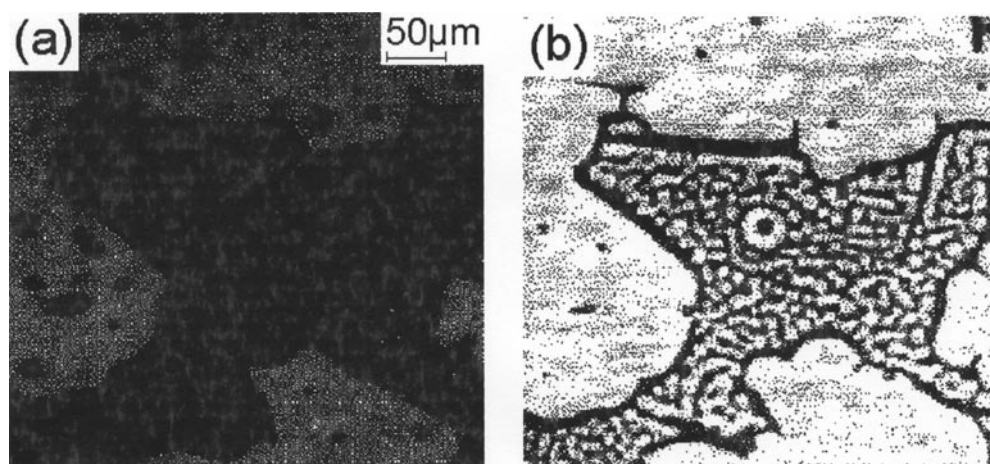
Figure 2. Optical micrograph of a patch of 8CB in the vicinity of the nematic–isotropic phase transition. (a) Temperature slightly below the phase transition temperature; (b) at the phase transition (same patch as in (a)). For temperatures above the phase transition temperature, the film spreads again to the appearance as in (a). Upon cooling again, the same transient dewetting phenomenon occurs.

by the strong cohesion resulting from the long-range dipolar forces. It is therefore not surprising that thick films can be generated on the Langmuir trough, given the high polarizability ($\epsilon \approx 80$) of the underlying water. In contrast, when the film is transferred onto the silicon wafer, the substrate polarizability is decreased roughly by a factor of 20, thus reducing the polar adhesion to the substrate considerably, with the possibility of dewetting by long-range forces [4].

Similar structures can, quite unexpectedly, also be observed in LC films which wet the surface completely, albeit not as an equilibrium morphology. In figure 2, we show a patch of octyl-cyano-biphenyl (8CB) which had been deposited by spin casting from hexane solution and is approximately 80 nm thick. Figure 2(a) shows the smooth patch in the nematic state. Upon heating into the isotropic phase region, the patch undergoes, within seconds, a transition to the undulative state shown in figure 2(b), which is quite similar to the undulation from figure 1. However, as opposed to the structure observed with 5AB$_4$, the film becomes perfectly smooth again as soon as the material has become all isotropic. Furthermore, upon cooling back into the nematic state, qualitatively the same transient dewetting phenomenon occurs. We thus see that, despite the material wetting the substrate in either phase (nematic or isotropic), there is a transient dewetting instability which occurs close to the phase transition and which produces structures very similar to spinodal dewetting patterns.

In order to develop an idea of how this effect may come about, let us recall that in a thin film, a phase transition usually does not affect the whole film material at the same temperature. In contrast, it is quite common that the high temperature phase (the isotropic phase in this case) first develops at the free boundary of the film, and at the substrate boundary only at some higher temperature. As a common example, one may take the solid boundary layer usually present close to the solid substrate in thin films of simple liquids [11, 12]. We may thus quite safely assume that there is a finite temperature range in which there is a phase boundary in the film parallel to the substrate, the distance of which (to the substrate) is controlled by temperature.

Now consider the fate of a small perturbation, say, an indentation, of the free surface, when the phase boundary is close to that surface. If the indentation reaches the boundary, it exposes the low temperature phase (LTP) (cf figure 3). In general, the surface tension of the
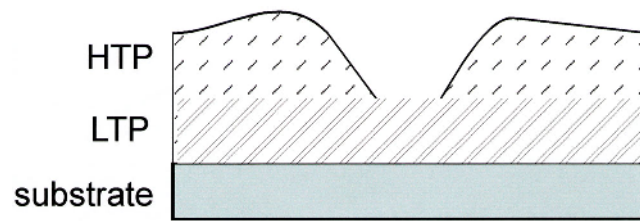
Figure 3. Sketch of the (possibly) Marangoni-type instability of transient dewetting in a LC film. HTP: high temperature phase (isotropic). LTP: low temperature phase (nematic).

LTP differs from that of the HTP, such that there is inevitably a surface tension gradient along the surface, which results in Marangoni flow in the film, i.e., to substantial material transport towards the regions with higher surface tension. A precondition for this to occur is, of course, that the film be liquid enough to sustain the transport; this is fulfilled in the case of a LC.

In a conventional fluid, the surface tension of the HTP (e.g. the melt) is usually inferior to the surface tension of the LTP (e.g. the solid). As a consequence, the indentation is immediately restored, and the film is stable. In a liquid crystal, however, this may not be so. In particular, the surface tension of the isotropic phase is, for all the LCs we studied, *larger* than that of the nematic phase. Hence, Marangoni flow renders the film dynamically unstable, and dewetting by unstable surface waves is to be expected, as observed. It should be noted that this instability cannot be easily described in the framework of the effective interface potential, since it is directly related to the creation or annihilation of one of the interfaces involved.

Once a liquid film has ruptured, either by nucleation or by unstable waves, it develops holes, i.e., free patches where the film material has been more or less completely removed from the substrate. This removed material must then accumulate into thicker regions around the holes, and the dynamical properties of these structures are decisive for the emergence of the final liquid structure. As a comparably tractable example, we discuss the evolution of a circular hole in a smooth film, generated by heterogeneous nucleation such as the nucleated free patches in figure 1. The material removed from the substrate upon generating the free patch accumulates in a circular rim at the boundary of the hole, and both the hole and the height of the rim slowly grow with time [13].

This is quite a symmetric situation, but it turns out not to be dynamically stable. This is demonstrated in figure 4, which shows an optical micrograph of a heterogeneously nucleated circular hole in a polystyrene film dewetting a hydrophobized silicon substrate after some time of growth. Obviously, the rim has become unstable and has decayed into a circular arrangement of isolated droplets which are being left behind as the hole grows further. This happens because the rim represents a toroidal liquid surface, which is similar to a cylindrical surface due to its high aspect ratio. A cylindrical liquid surface, however, is subject to the Rayleigh–Plateau instability which transforms the cylinder into a row of equidistant droplets, as is well known from the liquid jet. Similarly, the toroidal rim decays into a corona of droplets, as shown in the figure.

We already see from this representative, yet anything but complete, account of the hierarchy of instabilities in dewetting liquid films that there is a strong drive of such systems to generate structures on their own. Let us now discuss how, and to what extent, this drive may be tamed in order to create artificial liquid structures in a controlled and predictable way. A rather obvious application could be the design of liquid microchips which have, as a substitute to the common electric conduction lines, little channels which may carry chemical or biological agents.
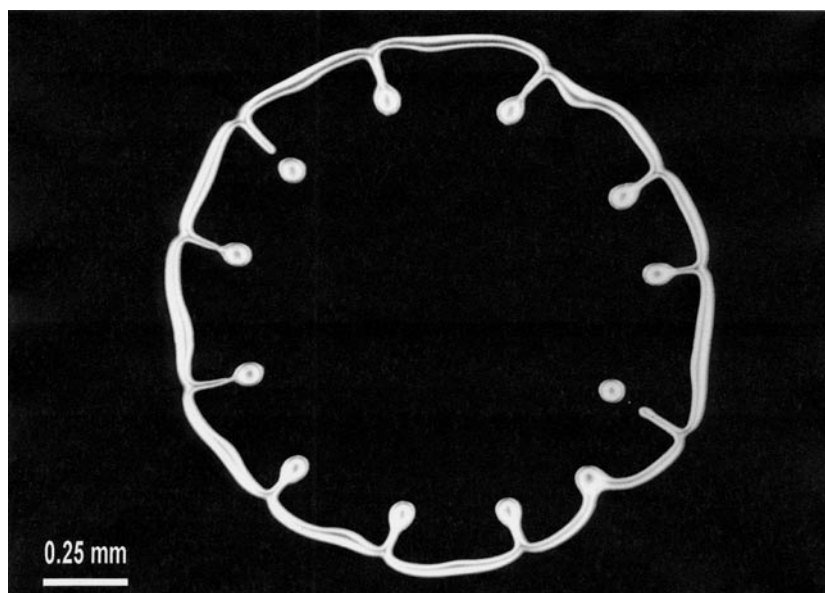
Figure 4. Instability of the rim of a circular hole which has formed in a 270 nm thick polystyrene (65 k) film at 130 °C, dewetting a silicon substrate which had been hydrophobized by treatment with octadecyl-trichloro-silane. The diameter of the hole is approximately 150 μm.

3. Controlling liquids at interfaces: wetting of artificially structured substrates

The central idea is to create a pattern of spatially varying wettability on the substrate in order to force the liquid into the desired shape. A rather simple way to do this is to evaporate, through a suitable mask, a poorly soluble salt, which renders the surface hydrophilic but does not appreciably dissolve in the adsorbed liquid. For demonstration, we have generated parallel wettable stripes on an elsewhere hydrophobic substrate by evaporating magnesium fluoride onto a silicone rubber surface using as a mask a commercial grid, which is available for transmission electron microscopy (purchased from the Plano company).

In order to deposit a liquid (water, in this case) onto this sample, we have mounted it onto a Peltier element and cooled it below the dew point. The result is shown in figure 5, where one can see parallel cylindrical channels of condensed water which have formed on the hydrophilic stripes. Virtually no droplets grew on the hydrophobic regions, which is a result of the proximity of the cylindrical channels: the latter have a much smaller curvature and thus a smaller saturation pressure. Hence they win the competition for the condensing water against the small droplets nucleating between them, thus keeping the latter from growing†. It is therefore essential for the experiment that the wettability pattern be on a microscopic scale. Trying this with millimetre-sized structures would be quite a mess.

It is interesting to note that the channels displayed in figure 5 are stable, even though they represent cylindrical liquid surfaces. The reason lies in the fact that their contact lines are pinned to the boundaries of the hydrophilic regions. To demonstrate this, let us discuss the fate of a liquid current fluctuation along a channel. It is quite obvious from the section sketched in figure 6 that when the contact angle, θ, of the liquid at the boundary of the hydrophilic region

† This can be seen also in figure 9. Numerous droplets condense on the sample, but in close proximity of (mostly between) the channels, their density is greatly reduced.
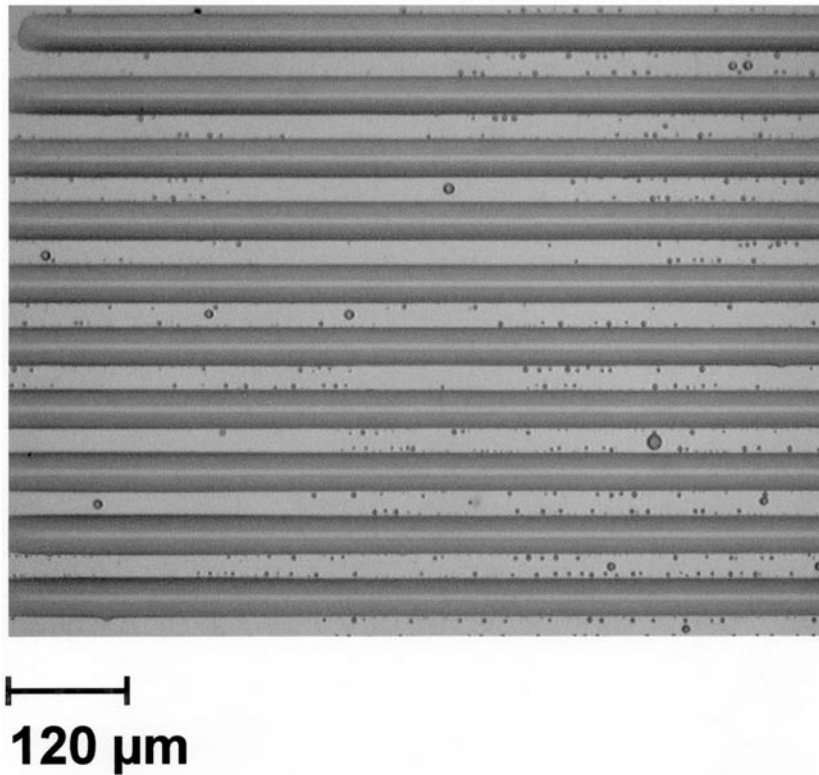
120 µm

Figure 5. Parallel cylindrical channels of condensed water which have formed on hydrophilized stripes on an elsewhere hydrophobic (silicone rubber) surface.
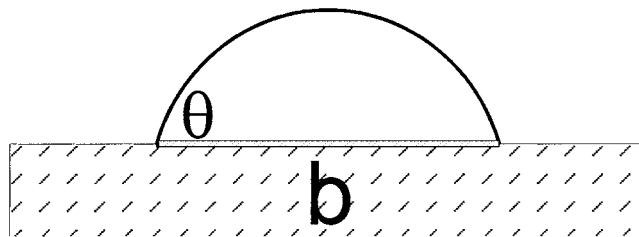

Figure 6. Sketch of the cross section of a channel like those in figure 5. The liquid surface is pinned to the boundaries of the hydrophilic domain, where it forms a contact angle, Θ, with the substrate. b denotes the width of the hydrophilic domain.

is below $90°$, the radius of curvature of the liquid surface will decrease if liquid is accumulated there. Since the Laplace pressure in the channel is given by σ/R (σ being the surface tension and R the radius of curvature), this results in an increase in pressure which repels the liquid from this place and thus restores the fluctuation. Hence, the cylinder is stable.

Conversely, if the contact angle is larger than $90°$, accumulation of liquid in a certain region of the channel results in an increase in the radius of curvature, and thus a decrease in Laplace pressure. As a consequence, even more liquid will accumulate there, i.e., the channel is unstable. In fact, figure 7 shows the same sample as in figure 5, after some more water had
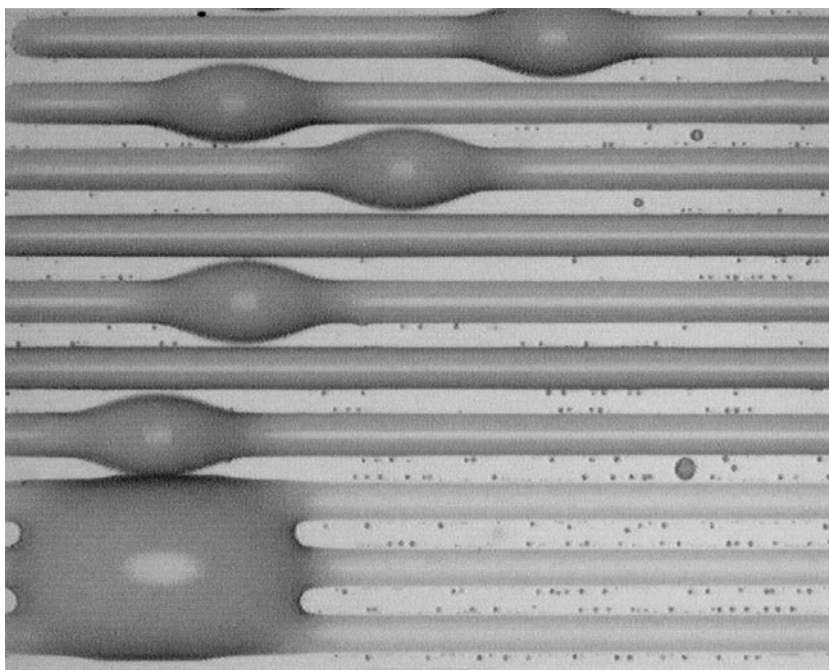
120 µm

Figure 7. Same sample as in figure 5, but after deposition of more water. The channels have become unstable, forming one droplet per channel. Two such droplets have merged to create a bridge.

condensed onto the stripes. It is clearly seen that droplets have now developed, but as opposed to the well-known periodic droplet ensemble emerging in the Rayleigh–Plateau instability of a free cylinder, there is only one droplet per channel.

This can be understood if one derives the spectrum of the fluctuations. This can be obtained from the Stokes equation for the current along the channel, which is easily solved for small perturbation amplitudes by harmonic mode analysis. It turns out that, just as in most dynamical instabilities, there is one mode for which the amplitude grows the fastest, and this is expected to dominate the emerging structure. In figure 8, the wavelength of this fastest mode is plotted as a function of the contact angle. As discussed above, there is no instability below $\theta = 90°$. For larger θ, there is a characteristic spectrum which displays a pole at $90°$ from above. In the experiment, water condenses gradually, and the contact angle is thus gradually increased until it crosses the border of stability at $\theta = 90°$, just where the critical wavelength is infinite. As a consequence, since the length of the channels is finite, there will only be one droplet per channel.

To corroborate experimentally that the boundary of stability lies at $\theta = 90°$, we have varied the hydrophobicity, and thus the advancing contact angle (ACA) of water on the silicon rubber substrate by treating it with a plasma discharge for variable exposure times. While for ACAs above $90°$ the instability was consistently observed, for ACAs below $90°$ the channels instead
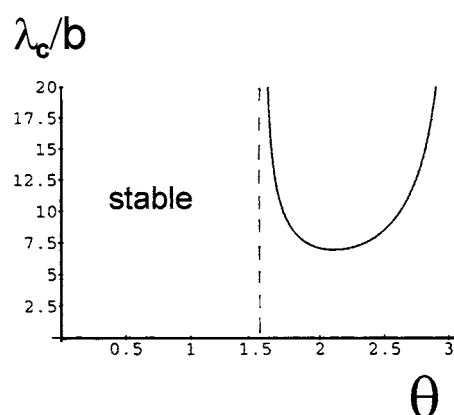
Figure 8. The wavelength, measured along the channel, of the fastest growing fluctuation mode as a function of the contact angle. At $\Theta = 90°$, where the channels cross from the stable to the unstable regime, the wavelength is infinite, thus creating only one droplet per channel.

spread gradually onto the hydrophobic regions of the substrate. This is in perfect agreement with the above model, since the actual contact angle at the boundary of the hydrophilic region will never exceed the ACA on the adjacent hydrophobic domain.

We see that while providing a wettability pattern on the substrate helps to guide the liquid into a desired shape, there are still interesting effects which take place on a self-organized basis. Let us see what happens if we leave the simple shape of straight lines, as shown in figure 5, and instead investigate the 'corners', as those displayed in figure 9. They represent the simplest generalization of the above channels on the way to a 'liquid chip', and have been generated in just the same way as the channels discussed above, only the mask is now custom-made.

The five corners shown have in common the width and length of the channels attached to them, but differ only in their width in the corner region. This width, denoted by w, increases from channel a to channel e. When the sample is cooled at ambient atmosphere such that water condenses and gradually fills the channels, the behaviour of the emerging liquid structures is found to distinctly depend on w. When w is large (e), the corner is also filled gradually, developing a drop which is localized at the corner. In an intermediate range (b–d), the corner first has an appearance similar to the adjacent channel, but is suddenly and discontinuously filled with a drop when a certain Laplace pressure is reached. It is easy to imagine that putting an additional channel with its end close enough to such a corner will result in a kind of valve which is closed by the drop bridging the corner to the additional channel. It may be controlled by the total amount of liquid, or by the Laplace pressure of the system.

However, this represents a rather poor control on the liquid structures. Another and more accessible way of control consists of employing two (instead of one) patterned substrates, put in close proximity to each other, such that the liquid does not only need to be arranged in accordance with one substrate, but with both. Figure 10 shows a sketch of two such patterned surfaces, between which liquid channels form wherever hydrophobic domains are opposing each other. It is clear that the distance of the substrates must be below a certain critical value, because otherwise the surface tension of the liquid, the influence of which is proportional to the distance of the substrates, will favour the formation of a single liquid object instead of a number of separate ones. This critical distance is on the order of the spacing of the hydrophilic lines, with some dependence on the geometry of the pattern and its contrast in wettability.
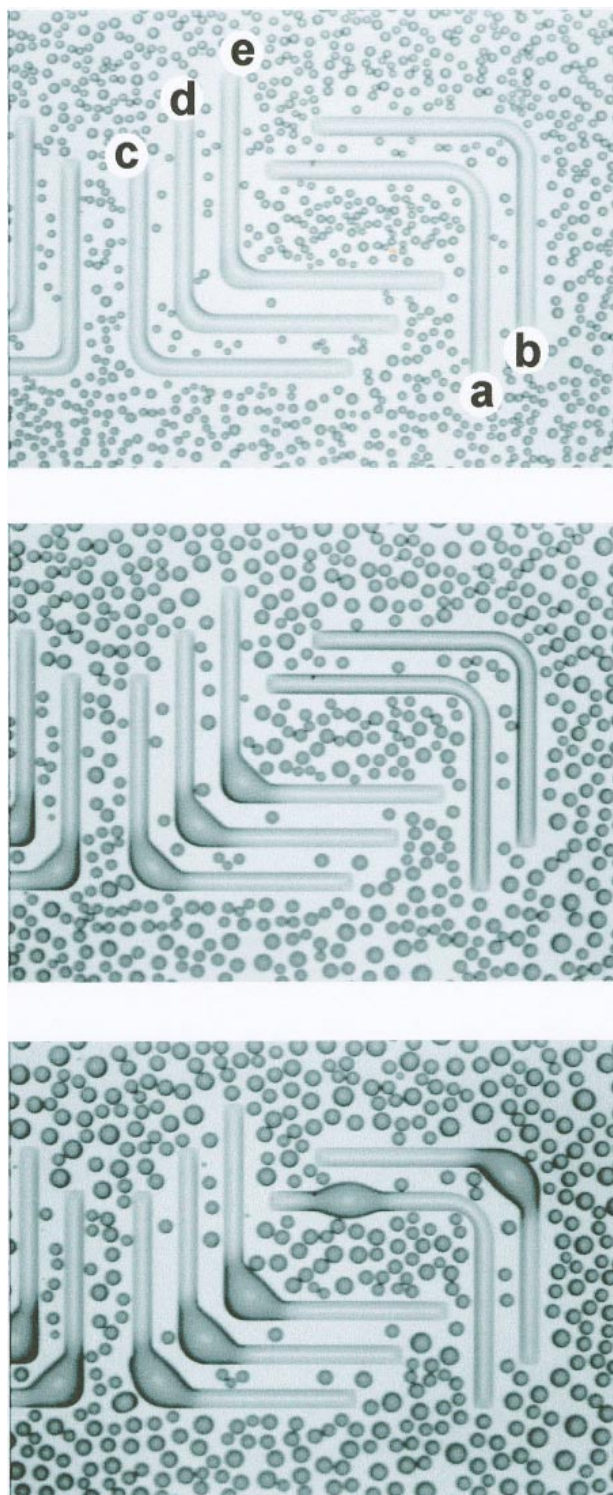
Figure 9. Deposition of water onto wettable 'corners'. Time (and thus the adsorbed volume) increases from top to bottom.
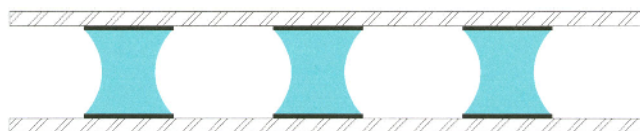
Figure 10. Sketch of two opposing substrates bearing a wettability pattern, with some liquid in between them. It is clear that their distance must not exceed a certain critical value in order for such a liquid structure to form.
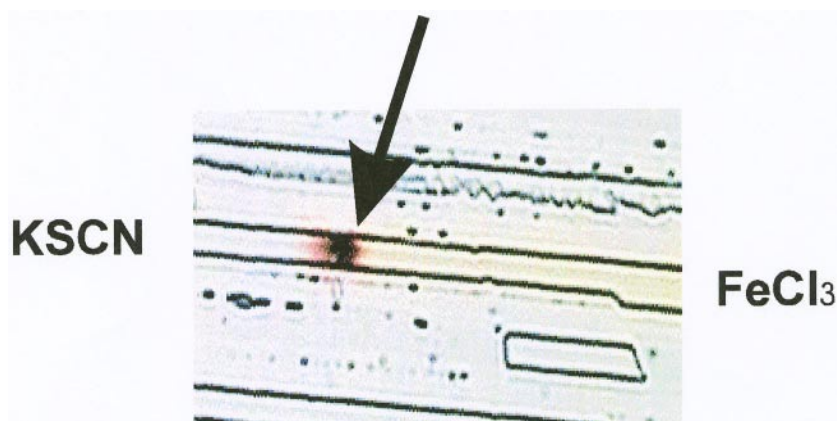

Figure 11. A chemical reaction in a liquid channel of the kind sketched in figure 10. From above, the channel is filled with an aqueous solution of $FeCl_3$, with KSCN from below. The arrow indicates where the chemical reaction has started.
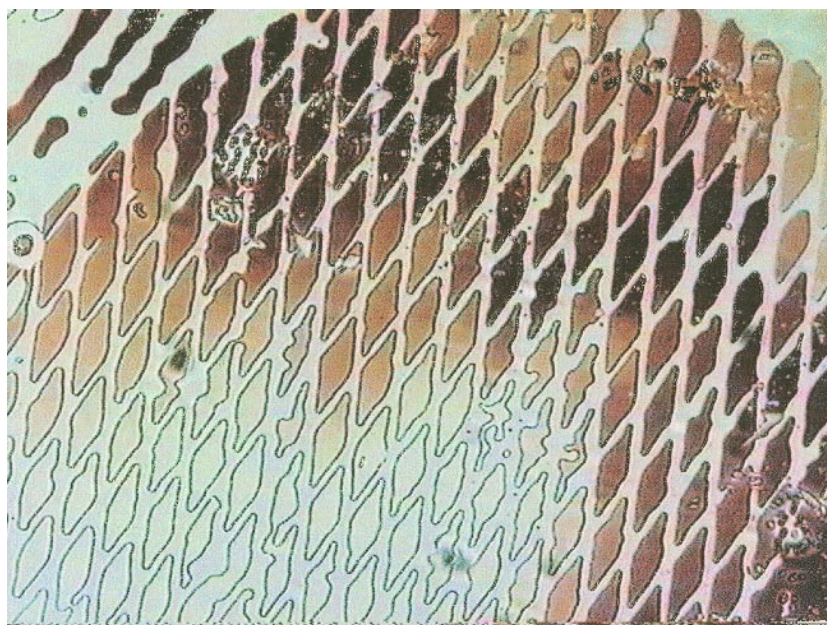

Figure 12. Some azimuthal tilt of the substrates with respect to each other leads to the formation of isolated compartments, here with different dye concentrations. By laterally shifting one of the substrates, the compartments can be effectively moved on the sample.

To demonstrate this concept, we show in figure 11 a channel which has formed between two substrates in the way described, and which has been filled from both sides with aqueous solutions of $FeCl_3$ and KSCN, respectively, which react at the centre of the image (arrow) to yield a dark red precipitate. One can follow this micro-compartment reaction in detail, as the reactants diffuse towards each other, and the product diffuses away. Many isolated compartments are formed when the two substrates are given a finite azimuthal angle with respect to each other, as shown in figure 12. These can be effectively moved along the sample by lateral displacement of one of the substrates.

As we have seen, the drive of structure formation and shaping in liquids at solid interfaces lead to a variety of interesting phenomena, but can also be used to generate and control artificial liquid structures at the will of the experimentalist. In the next section, we will return to the basic research aspects of the matter and see how we can derive fundamental quantities of wetting science from thorough investigation of the profiles of such liquid structures.

4. Deriving fundamental quantities from liquid structure profiles

It was mentioned above that the artificial structures studied here are (and must be) small scale, and we have so far dealt with structures several microns in width. Let us now raise the question of how things change when we reduce the lateral scale by, say, two orders of magnitude. These structures can no longer be produced by evaporation through a mask, since free-standing masks with submicron lateral scale are not readily available. Instead, we have used the well-established method of micro contact printing (μCP) to generate patterns of self-assembled monolayers (SAMs) of hydrophobic compounds covalently bound to the substrate [14]. More specifically, we have used silicone rubber stamps cast from silicon masters to print patterns of perfluorinated alkyl silanes from hexane solution onto silicon substrates.

Figure 13 shows an AFM image (tapping mode) of such a pattern. The spatial period of the hydrophobic stripes in this case is 900 nm, their height is slightly less than the length of the molecules due to the finite tilt angle of the latter. It is remarkable how strongly this submicron pattern affects even droplets which are two orders of magnitude larger. This is demonstrated in figure 14, which shows an optical micrograph of droplets of hexaethylene glycol deposited on a substrate bearing a stripe pattern with 400 nm period. The faceting of the droplets in the stripe direction is clearly visible.

We are now interested in the interaction of the liquid drops with the substrate on the small scale of the wettability pattern. It is obvious that we will not be able to investigate this by optical microscopy, since this does not provide the required spatial resolution. However, it has been shown before that the surface profiles of even low viscosity liquids can be imaged by AFM in tapping mode without appreciable distortion, provided the imaging parameters are carefully adjusted [15–17]. Images of small droplets and the liquid profile at the three-phase boundary (contact line region) can thus be obtained with a resolution of a few nanometres. A typical image of a small droplet is shown in figure 15. As we will see below, images like this can now be used to determine the three-phase contact line tension, i.e., the excess free energy connected to the line at which the substrate, the liquid and the air meet.

Contact line tensions, usually denoted by τ, are probably the most controversial quantities in wetting science. The classical approach for their measurement is to investigate the dependence of the contact angle of small sessile droplets upon their size. The smaller a droplet becomes, the larger becomes the effect of the contact line tension on its shape. For a positive line tension, the droplet base is contracted, which gives rise to an increased value of the contact angle. This is expressed by the modified Young equation for a liquid droplet on a
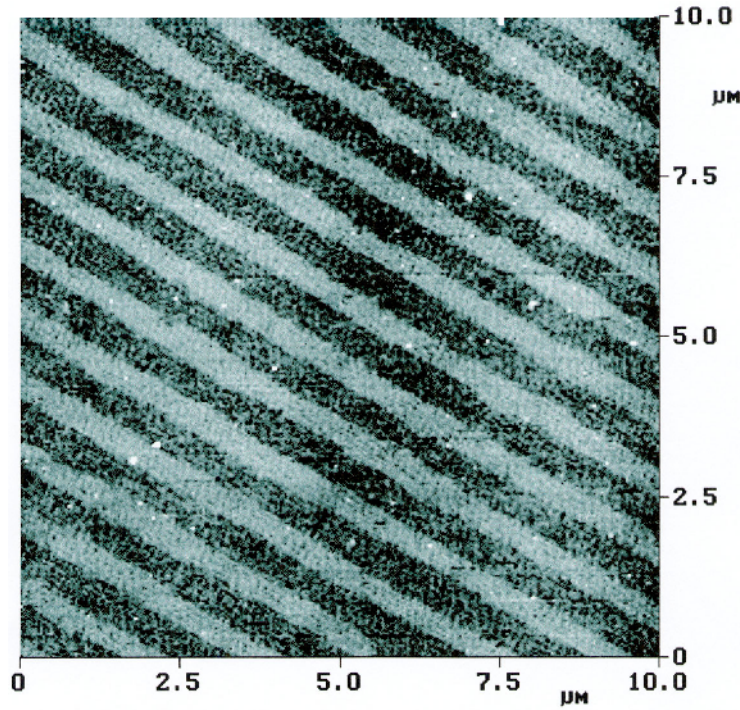
Figure 13. SFM topography image of a patterned silicon wafer. The stripes of self-assembled monolayers of perfluorinated monochloroalkylsilane (height: 0.5 nm) are prepared by μCP. A wettability contrast of hydrophilic (not-stamped) and hydrophobic (stamped) stripes is obtained (periodicity: 900 nm).

plane solid surface, which reads

$$\cos(\Theta) = \cos(\Theta_{Young}) - \frac{1}{\sigma}\frac{\tau}{R} \qquad (1)$$

where Θ is the actual contact angle the droplet forms with the substrate, and Θ_{Young} is the contact angle which would be derived from Young's equation (i.e. for a straight contact line, or infinitely large drop). R is the radius of the (circular) contact line. Experiments have been performed for a long time using optical techniques on droplets with typical sizes of at least several tens of micrometres. The results show an exceptionally large scatter in the magnitude of the contact line tensions obtained. Values ranging from 10^{-5} to 10^{-12} N, both positive and negative, are reported in the literature [18–22].

Theory predicts that the typical values of τ should be in the range of a few tens of piconewtons [23–29]. The characteristic length scale at which these forces become important can readily be obtained by comparison with typical values of interfacial tensions: $\tau/\sigma \approx 10^{-11}$ N$/10^{-2}$ N m$^{-1} = 1$ nm. At much larger scales, interfacial tensions are expected to dominate all measurements of line tension effects, and particular care must be taken in the experiments. High-resolution imaging of the three-phase contact line and the local liquid surface is thus crucial for the determination of the contact line tension. This is not easily possible with optical techniques due to the lack of spatial resolution, and we will show here that the problem can be tackled with AFM.

A close-up of the contact line region of a hexaethylene glycol droplet is shown in figure 16. Images (3 μm $\times$ 3 μm) obtained with $\approx$10 nm lateral resolution, were processed numerically

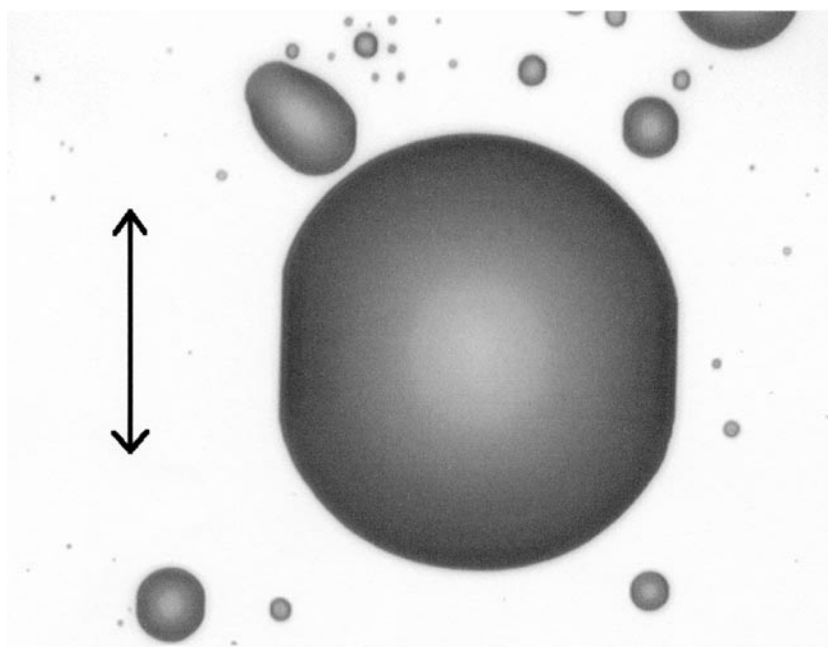**Figure 14.** An optical micrograph (150 μm $\times$ 110 μm) of hexaethylene glycol droplets deposited on a patterned substrate is shown. The underlying substrate with the stripes in the direction of the arrow drawn (periodicity: 400 nm) induces elongated droplets, even on the macroscopic scale.

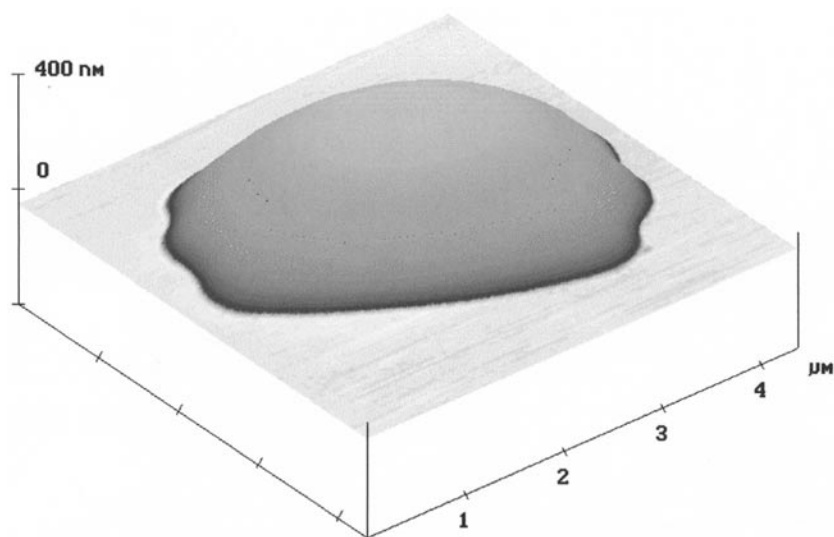**Figure 15.** SFM topography image of a small droplet on a patterned substrate (periodicity: 800 nm). The elongation of the droplet in the direction of the stripes and the distinct corrugation of the contact line perpendicular to the stripes can be clearly seen.

in order to obtain the local radius of curvature of the contact line and the local contact angle. The radius of curvature of the contact line was obtained by a second-order polynomial fit in the
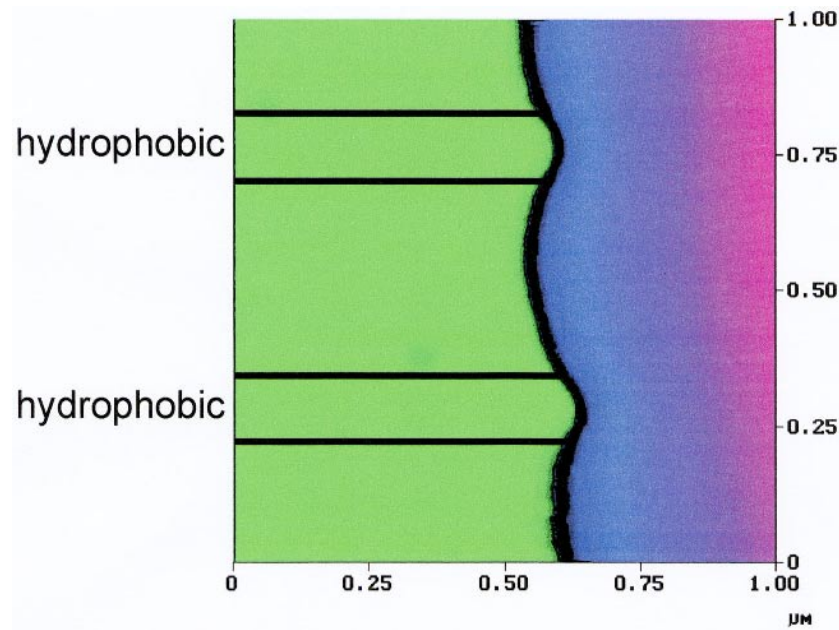
Figure 16. A high resolution (≈10 nm per pixel) SFM topography image of the contact line region of a large hexaethylene glycol droplet is shown. The corrugation of the contact line due to the stripewise wettability contrast of the substrate is used to determine the dependence of the local contact angle on the local curvature of the contact line. The direction of the stripes is from left to right in this image.
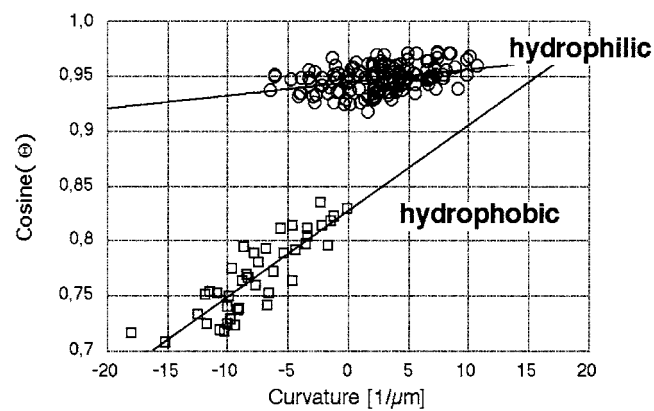

Figure 17. The experimental values of the cosine of the local contact angle are plotted versus the local curvature of the contact line. Two distinct clusters of data are seen, one at higher, and the other at lower cosines of the contact angle, corresponding to the hydrophilic and hydrophobic regions, respectively. A linear dependence of the cosine of the contact angle on the curvature of the contact line is observed, as expected from the modified Young equation (equation (1)). With a linear fit contact line tensions of -6×10^{-11} and -3.5×10^{-10} N for hydrophilic and hydrophobic surfaces, respectively, are determined.

vicinity of the point of interest along the contact line. The local contact angles were directly determined from the topographical data perpendicular to the local direction of the contact line.
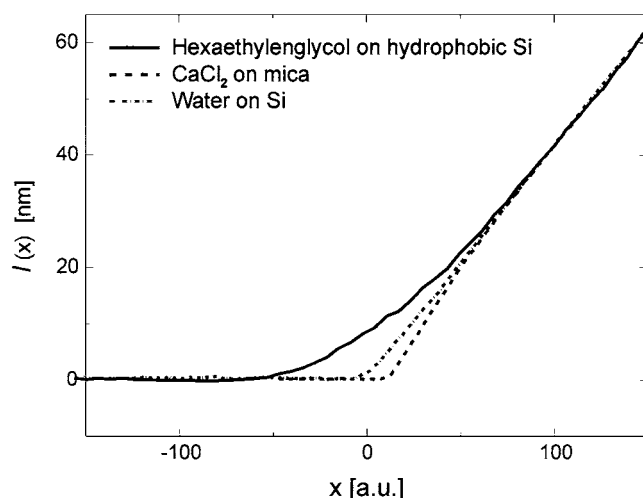
Figure 18. Liquid surface profiles close to the contact line for three different systems. From the shape of the profile we can derive the effective interface potential and the contact line tension. Results for the latter are in fair agreement with those values derived from the modulated contact lines via the modified Young equation.

In order to connect our data to equation (1), we have plotted the cosine of the contact angle Θ versus the local curvature of the contact line, $1/R$, in figure 17. As clearly seen, the data group into two distinct clusters, one at higher, and the other at lower cosines of the contact angle. They correspond to the hydrophilic (non-stamped) and hydrophobic (stamped) regions, respectively.

Quite obviously, the cosine of the contact angle varies linearly with the curvature of the contact line for both the hydrophilic and the hydrophobic domains. This dependency is expected from equation (1). It is now straightforward to determine the contact line tension by a linear fit, which is then found to be -6×10^{-11} N for the hydrophilic domains (Θ_{Young}: 18°), and -3.5×10^{-10} N for the hydrophobic domains (Θ_{Young}: 34°). By comparing our results with those of the above mentioned earlier experiments, one can see that the absolute values of the contact line tension are much lower, lying in the theoretically predicted range.

One can corroborate this result further by imaging the three-phase contact line of a droplet on a homogeneous substrate with even higher resolution. A close look reveals that the drop surface does not extend straight down to the substrate, but shows a slight distortion within a few tens of nanometres of the contact line. This can be seen from figure 18, which shows contact line profiles obtained for hexaethylene glycol on silicon, water on silicon, and calcium chloride solution on mica. In order to ease comparison of the profiles, the lateral scale has been normalized such that the liquid profiles approach asymptotically the same contact angle. As one can see, the profiles differ qualitatively from each other in the contact line region, which demonstrates that this is not an imaging artifact.

The shape of this distortion is determined by the effective interface potential, $\Phi(l)$, which describes the wetting forces acting between the liquid and the substrate. It is straightforward to derive $\Phi(l)$ from the profiles, $l(x)$, and it is also straightforward to compute the contact line tension from Φ [30]. It turns out that for hexaethylene glycol on silicon, we obtain in this way a line tension of minus a few tens of a nanonewton (with as yet very limited accuracy), in fair agreement with the result obtained from the undulative contact line on the patterned substrate.

This is remarkable insofar as the two ways of determining the line tension are completely complementary, and the fact that they have yielded comparable results must be considered as a good indication that the numbers obtained are quite reliable. We can thus hope that considerable insight into wetting phenomena on a nanometre scale will be gained by investigating liquid profiles by scanning force microscopy. Already the direct imaging of the contact line profile yields valuable information about the wetting forces at both long and short range, which are currently the subject of vivid discussions. In general, it seems that AFM-imaging of liquid surfaces may help to resolve long-standing debates about fundamental questions of wetting science.

5. Conclusions

We have seen that when a surface is exposed to a liquid by which it is not completely wetted, the liquid tends to generate a variety of structures upon beading off this surface. There is a whole hierarchy of dynamical instabilities leading from a homogeneous film to the final arrangement of individual droplets common for hydrophobic surfaces. By providing artificial patterns of wettability on the substrate, these forces may be used to generate liquid structures, which themselves exhibit interesting dynamical behaviour. Furthermore, we have shown that close examination of these artificial structures may yield valuable insight into the fundamental physical mechanisms of wetting and dewetting.

Acknowledgments

References

[1] Vrij A 1966 *Discuss. Faraday Soc.* **42** 23
[2] Ruckenstein E and Jain R K 1974 *Faraday Trans.* **II 70** 132
[3] Brochard-Wyart F and Daillant J 1990 *Can. J. Phys.* **68** 1084
[4] Herminghaus S *et al* 1998 *Science* **282** 916
[5] Sharma A and Jameel A T 1993 *J. Colliod Interface Sci.* **161** 190
[6] Khanna R and Sharma A 1997 *J. Colliod Interface Sci.* **195** 42
[7] Dietrich S 1988 *Phase Transitions and Critical Phenomena* vol 12, ed C Domb and J L Lebowitz (London: Academic)
[8] Schick M 1990 Introduction to wetting phenomena *Liquids at Interfaces* ed J Charvolin *et al* (Amsterdam: Elsevier)
[9] Ibn-Elhaj M, Möhwald H, Cherkaoui M Z and Zniber R 1998 *Langmuir* **14** 504
[10] Riegler R and Engel M 1991 *Ber. Bunsenges. Phys. Chem.* **95** 1424
[11] Rieutord F *et al* 1997 *Europhys. Lett.* **37** 565
[12] Herminghaus S, Paatzsch T, Häcker T and Leiderer P 1995 *Europhys. Lett.* **31** 157
[13] Jacobs K, Herminghaus S and Mecke K R 1998 *Langmuir* **14** 965 and references therein
[14] Xia Y, Mrksich M, Kim E and Whitesides G M 1995 *J. Am. Chem. Soc.* **117** 9576
[15] Fery A, Reim D and Herminghaus S 1997 *Ultramicroscopy* **69** 211
[16] Pompe T, Fery A and Herminghaus S 1998 *Langmuir* **14** 2585
[17] Fery A, Pompe T and Herminghaus S 1999 *J. Adhesion Sci. Technol.* **13** 1071
[18] Li D and Neumann A W 1990 *Colloids Surfaces* **43** 195
[19] Drelich J, Wilbur J L, Miller J D and Whitesides G M 1996 *Langmuir* **12** 1913
[20] Drelich J 1997 *Polish J. Chem.* **71** 525
[21] Aveyard R, Clint J H and Nees D 1997 *J. Chem. Soc. Faraday Trans.* **93** 4409

[22] Amirfazli A, Kwok D Y, Gaydos J and Neumann A W 1998 *J. Colloid Interface Sci.* **205** 1
[23] Marmur A 1997 *J. Colloid Interface Sci.* **186** 462
[24] Getta T and Dietrich S 1998 *Phys. Rev.* E **57** 655
[25] de Feijter J A and Vrij A 1972 *J. Electroanal. Chem.* **37** 9
[26] Harkins W D 1937 *J. Chem. Phys.* **5** 135
[27] Bresme F and Quirke N 1998 *Phys. Rev. Lett.* **80** 3791–4
[28] Rowlinson J S and Widom B 1984 *Molecular Theory of Capillarity* (New York: Oxford University Press) p 240
[29] Churaev N V, Starov V M and Derjaguin B V 1982 *J. Colloid Interface Sci.* **89** 16
[30] Indekeu J O 1992 *Physica* A **183** 439